Third Order Nonlinear Optical Characteristics of Er3+ doped BaMoO4 Nanostructures

RA sharath
SRMIST: SRM Institute of Science and Technology
K Mani rahulan (krahul.au@gmail.com)
SRM Institute of Science and Technology https://orcid.org/0000-0002-6003-3440
N Angeline Little Flower
SRMIST: SRM Institute of Science and Technology
annie sujatha
SRMIST: SRM Institute of Science and Technology
g vinitha
VIT University - Chennai Campus
Reshma Rajeev
SRMIST: SRM Institute of Science and Technology
tandrima saha
SRMIST: SRM Institute of Science and Technology
D Prakashbabu
SRMIST: SRM Institute of Science and Technology

Research Article

Keywords: Z-scan, erbium, nonlinear optical, saturable absorption

Posted Date: March 15th, 2021

DOI: https://doi.org/10.21203/rs.3.rs-289218/v1

Version of Record: A version of this preprint was published at Journal of Materials Science: Materials in Electronics on June 30th, 2021. See the published version at https://doi.org/10.1007/s10854-021-06476-3.

Third order nonlinear optical characteristics of Er^{3+} doped $BaMoO_4$ nanostructures

RA Sharath[a], K. Mani Rahulan [a*], N. Angeline Little Flower [a] , R. Annie Sujatha [a], G. Vinitha [b], Reshma Rajeev L[a], Tandrima Saha[a], D.Prakashbabu [c]

[a] *Nanophotonics Research Laboratory, Department of Physics & Nanotechnology, SRM Institute of Science & Technology, Kattankulathur, Chennai 603203, India*

[b] *Division of Physics, School of Advanced Sciences, Vellore Institute of Technology, Chennai 600048, India*

[c] *School of Applied Sciences, REVA University, Bangalore, Karnataka, 560 064, India*

Abstract

We report the third order nonlinear optical properties of Er^{3+}-doped $BaMoO_4$ nanostructures, and its dependence on Er dopant concentration. $BaMoO_4$ nanostructures with different concentration of Er were synthesized by chemical precipitation method and were characterized by UV-Vis absorption, X-ray diffraction (XRD), transmission electron microscopy (TEM) and fluorescence measurements. The incorporation of Er ions shifted the absorption band of $BaMoO_4$ towards higher wavelength and enhanced the light absorption in the visible region. XRD patterns showed that the powders crystallize in scheelite-type tetragonal structure. The nonlinear optical behavior of the nanostructures was investigated by a Z-scan technique at 532 nm using continuous wave Nd:YAG laser. Experimental results suggested that the addition of Er can considerably enhance the nonlinear absorption and refractive index coefficients of $BaMoO_4$ which could be used as a potential for nonlinear optical device applications.

Keywords: Z-scan, erbium, nonlinear optical, saturable absorption

*Corresponding author: K Mani Rahulan (krahul.au@gmail.com)

Foot note: ICONN-2021

1. Introduction

Research on nonlinear optical (NLO) materials exhibiting second and third order nonlinearities have been investigated for the development of next generation photonic devices. Materials displaying ultrafast response time and third order nonlinear susceptibility $\chi(3)$ are of great importance because of its various applications in signal processing, ultrafast optical switching devices, phase conjugation and optical bistability [1]. In recent years, numerous materials have been explored and fabricated for use in nonlinear optical devices.

In this regard, metal nanostructures have established significant attention owing to their exceptional NLO properties such as saturable absorption (SA), reverse saturable absorption (RSA), multiphoton absorption, self-focusing/defocusing effect arising from nonlinear refraction [2-4]. Molybdates has attracted the interest of several researchers due to its excellent optical properties which aids their wide use as laser materials, optic fiber, photoluminescent devices and scintillation detectors [5,6]. Report on NLO studies of molybdates crystals have shown to possess two photon absorption processes [7]. Our recent studies on NLO response of $CoMoO_4$ nanostructures have shown to exhibit excellent optical limiting behavior at 532 nm wavelength under pulsed (nanosecond) regime, rendering them ideal for optical limiting applications [8]. Among the various molybdate oxides, $BaMoO_4$ is one of the important materials used in the electro-optical industry due to its promising applications in solid-state lasers [9]. The inherent behavior of the $BaMoO_4$ can be tailored by adding suitable dopants to fit for the desired applications. Advanced hybrid materials are needed with high NLO properties for next generation optical technologies. In order to enhance the optical properties of $BaMoO_4$, erbium is used as a dopant due to its unique optical properties. Erbium doping with semiconductors can absorb light in infrared region makes them dual absorbers of UV and infrared light due to the transition between its discrete 4f levels (4I15/2 - 4I11/2) suitable for optical and photonic applications. Addition of Er^{3+} in $BaMoO_4$ nanostructures increases the efficiency on the basis of band gap tuning and probable luminescence upconversion. The optical properties are influenced by their structure, size and morphology. Even though the structural and optical properties of $BaMoO_4$ nanostructures were systematically investigated by researchers, its third order NLO properties still remains unexplored. Third order NLO properties of nanostructures have investigated by few researchers [10-12]. Here we report the linear and NLO properties of Er-doped $BaMoO_4$ nanostructures. Our experimental results show that the effect Er doping

enhanced the optical nonlinearity of the $BaMoO_4$ nanostructures. Our recent studies on the nonlinear optical characteristics of Er^{3+} doped with $SrMoO_4$ and $ZnWO_4$ have shown to possess enhanced optical nonlinearity with addition of Er [13,14].The structure and morphological characteristics of the materials are strongly dependent on the synthesis methods. Various methods have been explored for the synthesis of inorganic nanomaterials with improved structure and properties. Of the various techniques employed, chemical precipitation method has demonstrated to be an effective approach for synthesis. In the present study, pure and Er doped $BaMoO_4$ nanostructures with narrow size distribution have been prepared by a simple chemical precipitation method. The structure, morphology and optical properties of the $BaMoO_4$ samples were investigated. Furthermore, the nonlinear absorption coefficients of the nanostructures were extracted from the standard Z-scan technique achieved with continuous wave (cw) Nd:YAG laser at 532 nm. The data of real and imaginary parts of the third order NLO susceptibility $\chi(3)$ are extracted from both open and closed aperture measurements. Results indicates that NLO coefficients retrieved from the z-scan data are comparable with the previously reported $SrMoO_4$ and $ZnWO_4$ nanostructures, indicating the potential application of nanostructures for photonic applications.

2. Experimental section

2.1. Synthesis

The synthesis of pure and Er^{3+} doped $BaMoO_4$ nanostructures were performed at room temperature. In a typical experimental procedure, 1.48 g of $Ba(NO_3)_2.6H_2O$ and 1.00 g of $(NH_4)_6Mo_7O_{24}.4H_2O$ were dissolved separately in 50 ml of deionized water under stirring. Afterwards, the both solution was mixed together and the reaction was performed in an ultrasonic digestion system. Consequently, during sonication` different molar percent (0.3, 0.5, 0.7 and 0.9%) of $Er(NO_3)_3.6H_2O$ in aqueous solution was added to the above solution. After the reaction, the system was cooled to room temperature and the obtained precipitate was repeatedly washed with distilled water and then dried at 80ºC to yield the product. pure $BaMoO_4$ can also be synthesized using the same procedure without adding Er.

3. Results and discussions

3.1. X-ray diffraction (XRD) analysis

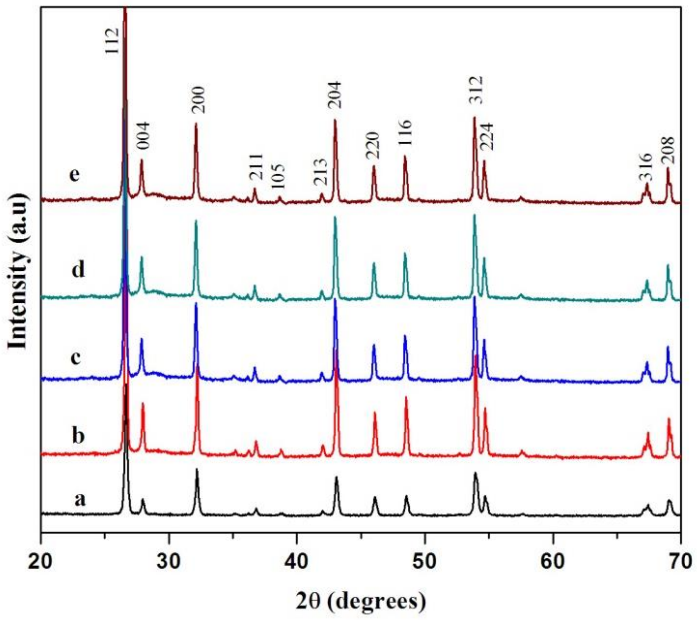

Fig. 1. XRD Pattern of Er^{3+} doped $BaMoO_4$ nanoparticles (a) pure (b) 0.3% (c) 0.5%, (d) 0.7% & (e) 0.9%Er

The structure and composition of Er^{3+} doped $BaMoO_4$ nanostructures were determined by XRD. Fig.1. Represents the XRD patterns of the $BaMoO_4$ with different concentrations of Erbium. All the samples exhibits scheelite- type crystalline structure and correspond to tetragonal phase of $BaMoO_4$ which are in good accordance with the standard reported data (JCPDS: 29-0193). The high intensity diffraction peaks related to the crystallographic planes (112), (004), (200) and (312) indicates the substantial growth in these planes. The strong and sharp diffraction peaks suggested the synthesized structures were well-crystallized. No diffraction peaks due to other impurities was detected. From the XRD spectra, it is suggested that the creation of charge difference by Er^{3+}doping into the site of Ba^{2+} did not influence the structural properties of $BaMoO_4$ [15,16].

3.2 Transmission Electron Microscopy (TEM)

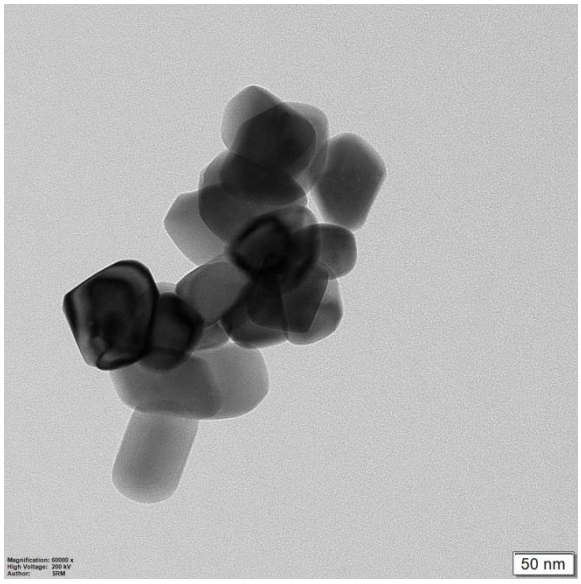

Fig. 2. TEM image of 0.5% Er^{3+} doped $BaMoO_4$ nanostructures

The morphologies and size of the Er^{3+} doped $BaMoO_4$ nanostructures were investigated by TEM. From the image shown in Fig. 2, it is observed that the particles tend to be agglomerated and have a size of about 55-60 nm. The particles are well dispersed and their size distribution is relatively narrow.

3.3. UV–visible Diffuse reflectance spectroscopy

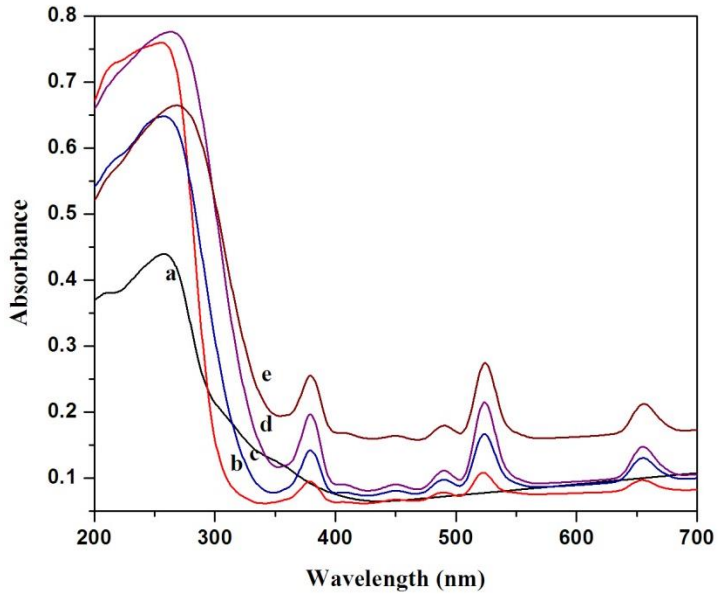

Fig. 3. UV-visible spectra of Er^{3+} doped $BaMoO_4$ nanostructures (a) pure (b) 0.3% (c) 0.5%, (d) 0.7% & (e) 0.9%Er

The room temperature absorbance spectra of Er^{3+} doped $BaMoO_4$ nanostructures are shown in Fig. 3. All the samples have shown fundamental absorbance maxima in UV range. It is seen that, the absorbance spectra gets red shifted corresponding Er^{3+} dopant concentration, thereby decreasing the band gap of $BaMoO_4$. Increasing Er concentration in $BaMoO_4$ leads to the creation of impurity bands which increases the donor-to-valence band of host material. The absorbance maxima appeared at 380, 488, 520 and 650 nm are due the 4f electronic transitions from $^4I_{11/2}$-$^2H_{9/2}$, $^4I_{15/2}$-$^4F_{7/2}$, $^{4I}_{15/2}$-$^2H_{11/2}$, and $^4I_{15/2}$-$^4F_{9/2}$ states of Er^{3+}, respectively [17-19]. The results indicate that the doping of Er^{3+} not apparently changes the band gap of nanostructures, but enhanced the light absorbance in visible region. The optical band gap energy (Eg) was calculated by the method proposed by Wood and Tauc [20]. According to this method, the Eg is accompanied with absorbance and photon energy by the following equation:

$$\alpha h\upsilon = A\,(h\upsilon - Eg)^n$$

where A is the absorbance, h is the Planck constant, υ is the frequency, Eg is the optical band gap and n is a constant associated to the different types of electronic transitions. Literature reports have shown that the molybdates have a typical optical absorption process governed by direct transitions. The optical band gap is calculated to be 4.17, 4.2, 3.87 & 3.17 eV for pure, 0.3, 0.5, 0.7 & 0.9 mol% of Er^{3+}-doped $BaMoO_4$ respectively.

3.4 Fluorescence measurements

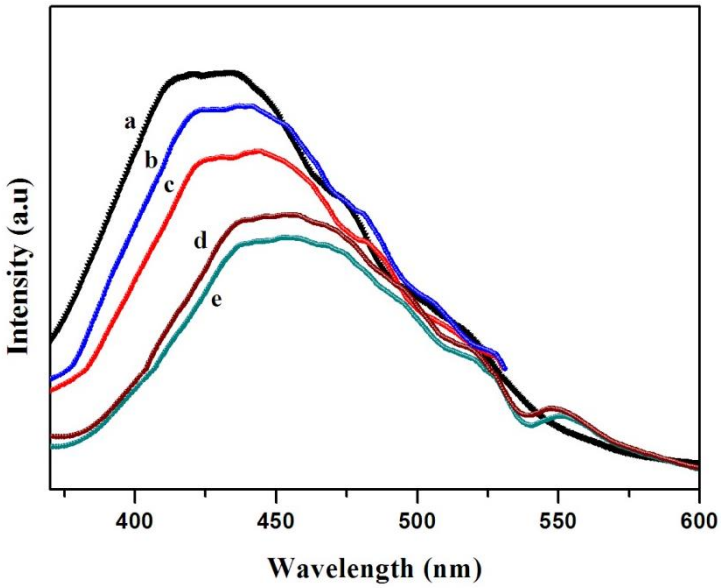

Fig. 4. Fluorescence spectra of Er^{3+} doped $BaMoO_4$ nanostructures (a) pure (b) 0.3% (c) 0.5%, (d) 0.7% & (e) 0.9%Er

The fluorescence spectra of Er^{3+}-doped $BaMoO_4$ nanostructures excited at a wavelength of 350 nm are shown in Fig. 4. The fluorescence emission of $BaMoO_4$ showed emission spectra at 422 nm, attributed to charge transfer transitions in $[MoO_4]^{2-}$ complexes with Td symmetry groups or self-trapping electronic states. All the samples have shown broad emission peaks due to the participation of several energy states within the bandgap which can act as trapping centers to trap electron populations. The fluorescence emission in $BaMoO_4$ is related to the distortion of $[MoO_4]$ tetrahedron complexes produced by the different angles between O-Mo-O [21]. The blue emission of molybdates is attributed to $^1T_2 \rightarrow {}^1A_1$ electron transitions into the $[MoO_4]$. The introduction of Er^{3+} decreases the emission intensity whereas the shape of the emission spectra remains unchanged. The reduction in emission intensity upon addition of Er^{3+} shortens the distance between two Er^{3+} ions leading to the formation of Er^{3+} clusters and increases the energy transfer process. In addition, a shift in the emission spectra towards higher wavelength is observed upon Er^{3+} doping, the red shift is due to the presence of impurity band generated from doping [22].

.

3.5. Nonlinear optical properties

The third order NLO properties of Er^{3+} doped $BaMoO_4$ with different concentration of Er has been investigated by a Z-scan technique developed by Sheik-Bahae et al [23]. Using a continuous laser (cw) Nd:YAG laser at 532 nm, the nonlinear absorption coefficient (β) and nonlinear refractive index (n_2) were determined from open aperture (OA) and closed aperture (CA) setup. The input intensity of the laser (I_0) was 1.435 kW/cm^2 and radius of the aperture (ra) was 1.5mm with the beam radius at aperture (ωa) measuring 3.5mm and focal length of lens -103 mm. The sample was dispersed in diethylene glycol and was taken in a 1mm cuvette and hence the path length is 1mm. The effective path length calculated came to be around 0.97mm. The CA Z-scan profile shown in Fig. 5 exhibits a prefocal transmittance peak before the focus and a post-focal transmittance valley after the focus. This shows that the samples possess negative nonlinear index with self-defocussing properties. Since, the cw laser source used in the study, the origin of such nonlinearity is attributed to thermal [24]. The absorption of cw laser causes a spatial distribution of temperature in the samples, producing a spatial variation of refractive index. This leads to thermal lensing effect resulting in severe phase distortion of the propagating beam [25]. The variation of thermal nonlinearity mainly arises due to the variation of Er dopant.

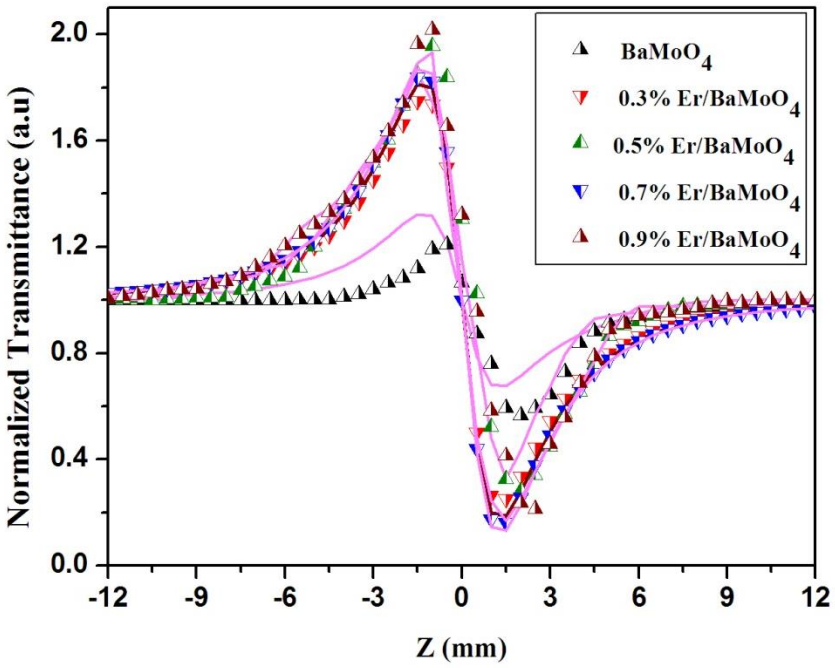

Fig. 5. Closed aperture Z-scan data of Er^{3+} doped $BaMoO_4$ nanostructures

The normalized transmittance for the CA Z-scan mode can be obtained theoretically with the following equation.

$$T_{CA}(\mathrm{Z}, \Delta\varphi_0) = 1 - \frac{4x\Delta\varphi_0}{(x^2+1)(x^2+9)}$$

Where Z is the sample position and $\Delta\varphi_0$ is the on axis phase shift at the focus.

Using the data acquired from the Z-scan, the nonlinear refractive index (n_2) was calculated from the difference between normalized valley and peak transmittance [26], given by

$$\Delta T_{P-V} = 0.406(1-S)^{0.25}|\Delta\varphi_0|$$

Where S is the linear aperture transmittance given by $S = 1 - \exp(-2r_a^2/\omega_a^2)$, r_a and ω_a represents the radius aperture and radius of the laser spot before the aperture. The phase change was calculated from the experimental peak valley value and the nonlinear refractive index was calculated using the relation [27].

$$n_2 = \frac{\Delta\varphi_0\lambda}{2\pi I_0 L_{eff}}(cm^2/W)$$

where λ is the incident beam wavelength and I_0 is the laser beam intensity at the focus (Z=0), L_{eff} is the effective sample thickness. The sample acts itself as a thin lens with varying focal lengths as it moves through the focal plane [28]. Fig. 6 shows the open aperture Z-scan curves of the samples. All the samples exhibit high transmittance value at the focus, confirms the occurrence of saturation absorption (SA). SA process involves the maximum transmittance of electromagnetic radiation at the focus as the samples moves towards the focal point. From the normalized OA Z-scan curves, the value of nonlinear absorption coefficient (β) has been determined using the relation.

$$\beta = \frac{2\sqrt{2}\cdot\Delta\mathrm{T}}{I_0\cdot L_{eff}}\ (cm/W)$$

The values of β and n_2 depend on the light–matter interaction that occurs when a laser of sufficiently high intensity is incident on a sample, and thus, the interaction can change the optical

properties of the medium. The normalized transmittance for the OA Z-scan mode can be obtained theoretically with the following equation.

$$T_{OA}(\mathrm{Z},\mathrm{S}=1)=\sum_{m=0}^{\infty}\left(\frac{[q_0(Z,0)]^m}{(m+1)^{3/2}}\right)$$

with $q_0=\frac{\beta I_0 L_{eff}}{1+Z^2/Z_0^2}$, $Z_0^2=2\pi\omega_0^2/\lambda$ is the Rayleigh range of the beam. The observed SA behavior of the nanostructures in present case is attributed to thermo-optic effects, due to the utilization of cw laser source [29]. During laser excitation all the available higher energy states are filled with photo generated carriers resulting in bleaching of carriers in the ground state. The accumulation of excited state carriers obstructs two or multi-photon absorption process and hence the transmittance increases when the samples was moved towards the focal point.

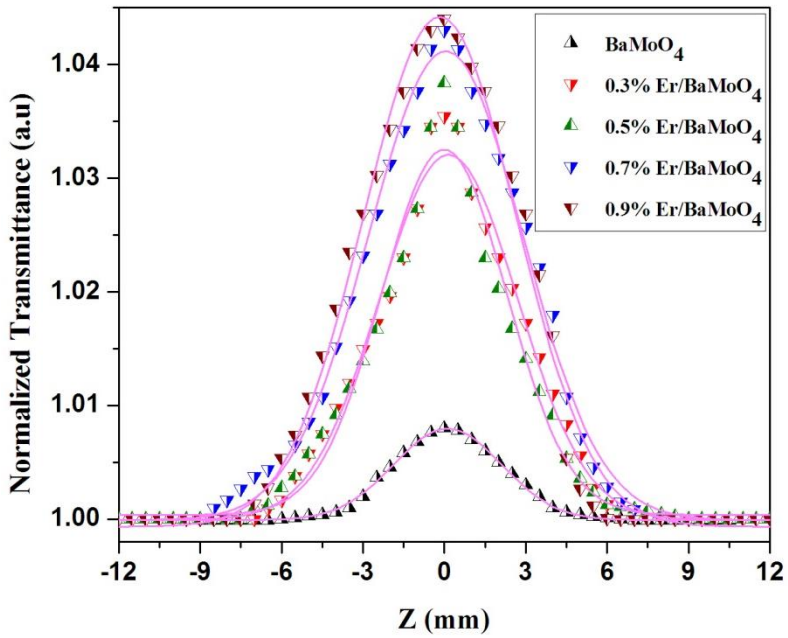

Fig. 6. Open aperture Z-scan data of Er^{3+} doped $BaMoO_4$ nanostructures

The real and imaginary parts of the third order nonlinear susceptility $\chi^{(3)}$ were determined from the nonlinear refractive index n_2 and nonlinear absorption coefficient β from the given equations [30]

$$Re\chi^{(3)}(esu) = 10^{-4}\frac{\varepsilon_0 c^2 n_0^2}{\pi} n_2(cm^2/W)$$

$$I_m\chi^{(3)}(esu) = 10^{-2}\frac{\varepsilon_0 c^2 n_0^2 \lambda}{4\pi^2}\beta(cm/W)$$

where ε_o is permittivity of the vacuum, n_o is the linear refractive index of the sample, and C is the velocity of light in vacuum. In all the samples, the real part of the third order nonlinear susceptibility is larger than the imaginary part, indicating the nonlinearity is dominated by nonlinear refractive behavior. The absolute value of third order nonlinear optical susceptibility can be calculated from the equation [31]

$$\chi^{(3)} = [(Re(\chi^3))^2 + Im(\chi^3)^2]^{1/2}$$

The calculated values of nonlinear refractive index (n_2), absorption coefficient (β) and third order nonlinear optical susceptibility $\chi^{(3)}$ are presented in the Table 1. Surface chemistry and material structure can influence the NLO properties. Under cw laser, the contribution of physical process can be due to electronic polarization, photorefractive effects, molecular orientation and thermal effects. $BaMoO_4$ nanostructures exhibited better nonlinear refraction value compared to the other reported NLO materials like azo dyes (0.54 x10 $^{-8}$ cm^2/W) [32], zinc sulphate (1.38 x 10 $^{-8}$ cm^2/W) [33], gold nanoparticles (2.23 x10 $^{-8}$ cm^2/W) [34], $CuNb_2O_6$ (5.16 x10 $^{-8}$ cm^2/W) [35]. The NLO properties of $BaMoO_4$ nanostructures are clearly dependent on the doping concentrations of Er which were evidently increased when the doping concentration of Er is increased. The increase in the strength of SA is due to the larger defect concentration and phase segregation caused by the Er ion doping into the $BaMoO_4$ host. The defect sites can act as carrier trapping centers and thereby decreasing the excitonic recombination rate. This leads to the ground state bleaching effect and promoting an increase in transmittance of the doped samples. The enhancement of nonlinear behavior is caused by free career absorption originated from the 4f shell transition in the Er^{3+} ions. Since Er^{3+} ions possess high polarizability and low cations field strength, the increment of nonlinear refractive index is strongly influenced by the addition

of erbium. The high polarizability of Er^{3+} ions leads to increasing number of the nonlinear refractive index. Therefore, it is clear that a contributing factor in the value of NLO parameters is influenced by the Er concentration of the material.

Table 1

Comparison of nonlinear optical parameters of pure and Er^{3+} doped $BaMoO_4$ nanoparticles

Samples parameters	**$BaMoO_4$**	**0.3 Er**	**0.5 Er**	**0.7 Er**	**0.9 Er**
Nonlinear refractive index, n_2 ´ 10^{-8} cm^2/W	3.62	8.58	9.49	9.909	10.34
Nonlinear absorption coefficient, β ´ 10^{-4} cm/W	0.0064	0.028	0.031	0.035	0.037
Real part of third order nonlinear refractive index Re $\chi^{(3)}$ ´ 10^{-6} esu	3.396	8.032	8.939	9.317	10.02
Imaginary part of third order nonlinear refractive index, Im $\chi^{(3)}$ ´ 10^{-6} esu	0.039	0.177	0.196	0.219	0.23
Third order nonlinear optical susceptibility, $\chi^{(3)}$ ´ 10^{-6} esu	3.396	8.034	8.941	9.319	10.03

Conclusion

Pure and Er^{3+}doped $BaMoO_4$ nanostructures was prepared by chemical precipitation method and their nonlinear optical behavior was studied. X-ray diffraction results showed that the synthesized materials formed scheelite- type structure and crystallized in tetragonal lattice. The inclusion of Er in $BaMoO_4$ is confirmed by fluorescence quenching. The third order nonlinear absorption and nonlinear refractive index of the nanostructures with different dopant concentration of Er have been investigated by Z-scan technique at 532 nm. Experimental result demonstrated that both pure and Er^{3+} doped nanostructures exhibit negative nonlinear refractive index. It is observed that the samples have shown enhanced nonlinear optical values of β, n_2 and $\chi^{(3)}$ than pure $BaMoO_4$. All these results suggested that the investigated nanostructures are potential candidate for nonlinear optical device applications.

Acknowledgement

This manuscript is part of the special issue of selected papers from the 6th edition of biennial International Conference on Nanoscience and Nanotechnology (ICONN-2021)

References

[1] L. Pan, N. Tamai, K. Kamada, S. Deki, Appl. Phys. Lett. 91 (2007) 051902.

[2] H.I. Elim,J.Yang,J.Lee, Appl.Phys.Lett.88(2006)083107.

[3] O.M. Folarin, E.R. Sadiku, A.Maity, Int.J.Phys.Sci.6(21)(2011)4869–4882.

[4]R.A. Ganeev, M. Suzuki, M. Baba, M. Ichihara, H. Kuroda, J. Appl. Phys. 103(2008)063102.

[5] Y. Sun, J.Ma, J.Fang, C.Gao, Z.Liu, Ceram.Int.37(2) (2011) 683–686.

[6] Mehdi Bazarganipour, Ceramics International, 42, (2016) 12617-12622

[7] T. T. Basiev, A. Ya. Karasik, A. A. Sobol', D. S. Chunaev, and V. E. Shukshin, Quantum Electronics **41** (4),370 (2011).

[8] K.Mani Rahulan, N. Angeline Little Flower, R. Annie Sujatha, N Padmanathan, C. Gopalakrishnan,Journal of Materials Science: Materials in Electronics 29 (2), (2018) 1504–1509

[9]A.P.A. Marques, D.M.A. de Melo, E. Longo, C.A. Paskocimas, P.S. Pizani, E.R. Leite, J. Solid State Chem. 178 (2005) 2346–2353.

[10] Mohd. Shkir, Mohd Taukeer Khan, V. Ganesh, I.S. Yahia, Bakhtiar Ul Haq, Abdullah Almohammedi, Parutagouda Shankaragouda Patil , Shivaraj R. Maidur, S. AlFaify Optics and Laser Technology 108 (2018) 609–618

[11] S. Arun Kumar, J. Senthilselvana , G. Vinitha, Optics and Laser Technology 109 (2019) 561–568

[12] K.Vasudevan, M.C.Divyasree, K.Chandrasekharan, Optics & Laser Technology 114 (2019) 35-39

[13] K. Mani Rahulan, Angeline Little Flower, N. Padmanathan, Anmol Mahendra,
Vijay Shekhawat, G. Vinitha, R. Annie Sujatha, M.A. Shivkumar, Journal of Photochemistry & Photobiology A: Chemistry 386 (2020) 112128

[14] R. Annie Sujatha, N. Angeline Little Flower, G. Vinitha, R.A. Sharath, K. Mani Rahulan, Applied Surface Science 490 (2019) 260–265

[15] Paramananda Jena, N. Nallamuthu, M. Venketswarulu, N. Satyanarayana, Ceram. Int. 40 (2014) 2349.

[16] R. Adhikari, J. Choi, R. Narro-Garcia, E. De la Rosa, J. Solid State Chem. 216 (2014) 36

[17] Liang Y, Sun K, Wang W, Chui P, Sun X. Mater Lett 2012;79:125–7.

[18] Chen G, Wang Y, Zhang J, Wu C, Liang H, Yang H. J Nanosci Nanotechnol 2012;12:3799–805.

[19] Rajesh Adhikari, Gobinda Gyawali, TaeHoKim, Tohru Sekino , Soo Wohn Lee, Materials Letters 91 (2013) 294–297

[20] Thongtem T, Kungwankunakorn S, Kuntalue B, Phuruangrat A, Thongtem S. J Alloy Compd, 506 (2010) 475−481.

[21] Yun-fei Liu, Li-li Xia, Yi-nong Lu, Shen-hua Dai, Masaki Takeguchi, Hui-min Hong, Zhi-gang Pan, Journal of Colloid and Interface Science 381 (2012) 24–29

[22] M.N. Azlan, M.K. Halimah and H.A.A. Sidek, Journal of Luminescence 181, (2017) 400-406

[23] M. Sheik-Bahae, A.A. Said, E.W. Van Stryland, High sensitivity single beam n_2 measurements, Opt. Lett. 14 (1989) 955–957.

[24] Rita S. Elias, Qusay M.A. Hassan , H.A. Sultan , Ahmed S. Al-Asadi , Bahjat A. Saeed , C.A. Emshary Optics and Laser Technology 107 (2018) 131–141

[25] M.D. Zidan, A. Arfan, A. Allahham, Optic Laser. Technol. 89 (2017) 137–142.

[26] M. Mashayekh, D. Dorranian, Size-dependent nonlinear optical properties and thermal lens in silver nanoparticles, Optik Int J Light Elec Opt 125 (2014) 5612–5617.

[27] Haider Mohammed Shanshool, Muhammad Yahaya,Wan Mahmood Mat Yunus, Ibtisam Yahya Abdullah, Opt Quant Electron 49 (2017)18

[28] R. Zakaria, M. H. Mezher, W. Y. Chong, Appl. Phys. A (2016) 122:664

[29] K.M. Sandeep, Shreesha Bhat, S.M. Dharmaprakash, Optics and Laser Technology 102 (2018) 147–152

[30] M. Krishnakumar, S. Karthick, K. Thirupugalmani, B. Babu, G. Vinitha, Optics and Laser Technology 101 (2018) 91−106

[31] M. Dehghanipour, M. Khanzadeh, M. Karimipour, M. Molaei, Optics and Laser Technology 100 (2018) 286–293

[32] C. Gayathri, A. Ramalingam, Spectrochem. Acta A 69 (2008) 980–984.

[33] Z. Dehghani, S. Nazerdeylami, E. Saievar-Iranizad, M.H.M. Ara, Synthesis and investigation of nonlinear optical properties of semiconductor ZnS nanoparticles, J. Phys. Chem. Solids 72 (2011) 1008–1010.

[34] Tingjian Jia, Tingchao He, Pengwei Li, Yujun Mo, Yuting Cui, A study of the thermal-induced nonlinearity f Au and Ag colloids prepared by the chemical reaction method, Opt. Laser Technol. 40 (2008) 936–940.

[35] N. Priyadarshani, G. Vinitha, T.C. Sabari Girisun, Optics and Laser Technology 108 (2018) 287–294

Figures

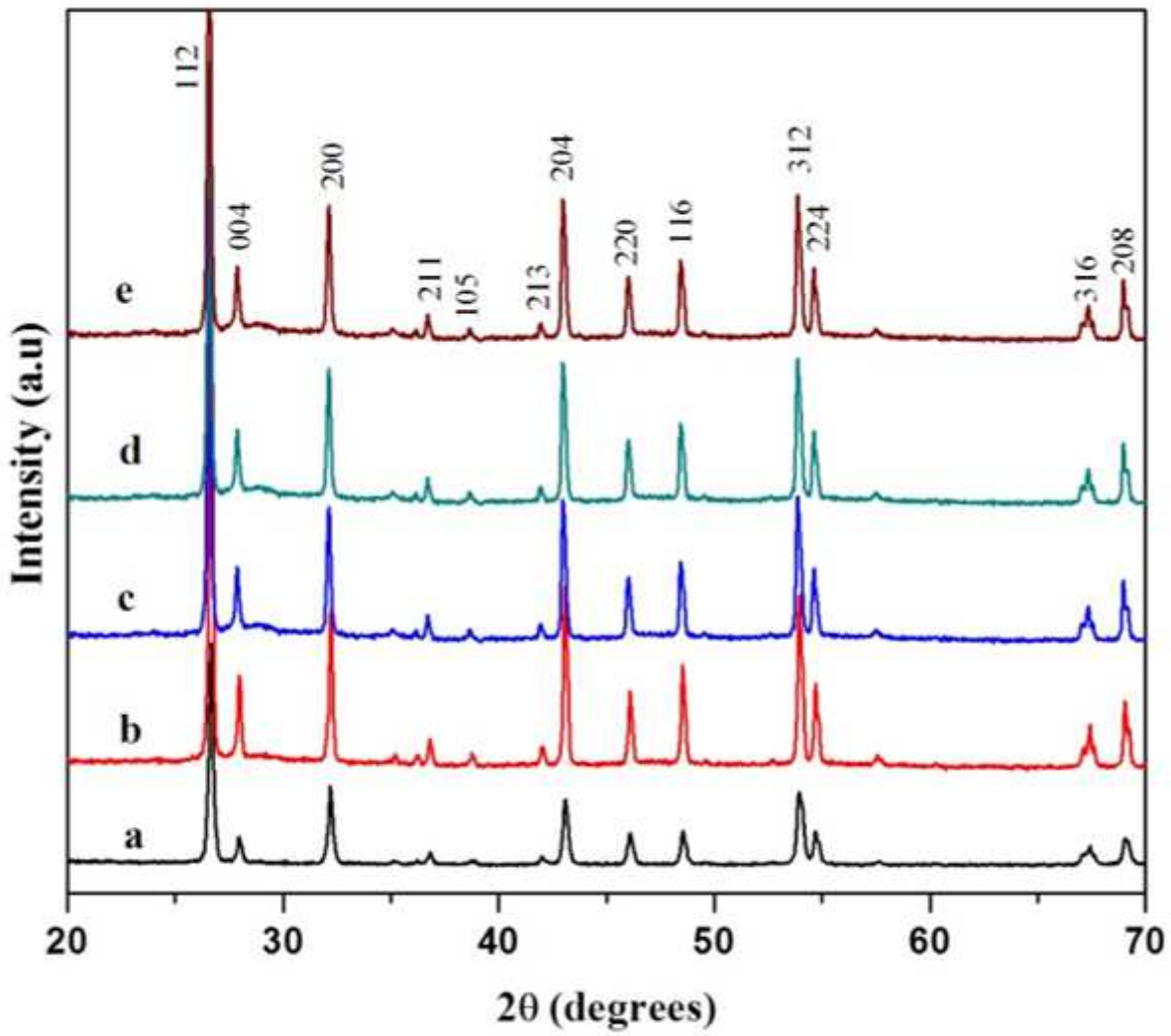

Figure 1

XRD Pattern of Er3+ doped BaMoO4 nanoparticles (a) pure (b) 0.3% (c) 0.5%, (d) 0.7% & (e) 0.9%Er

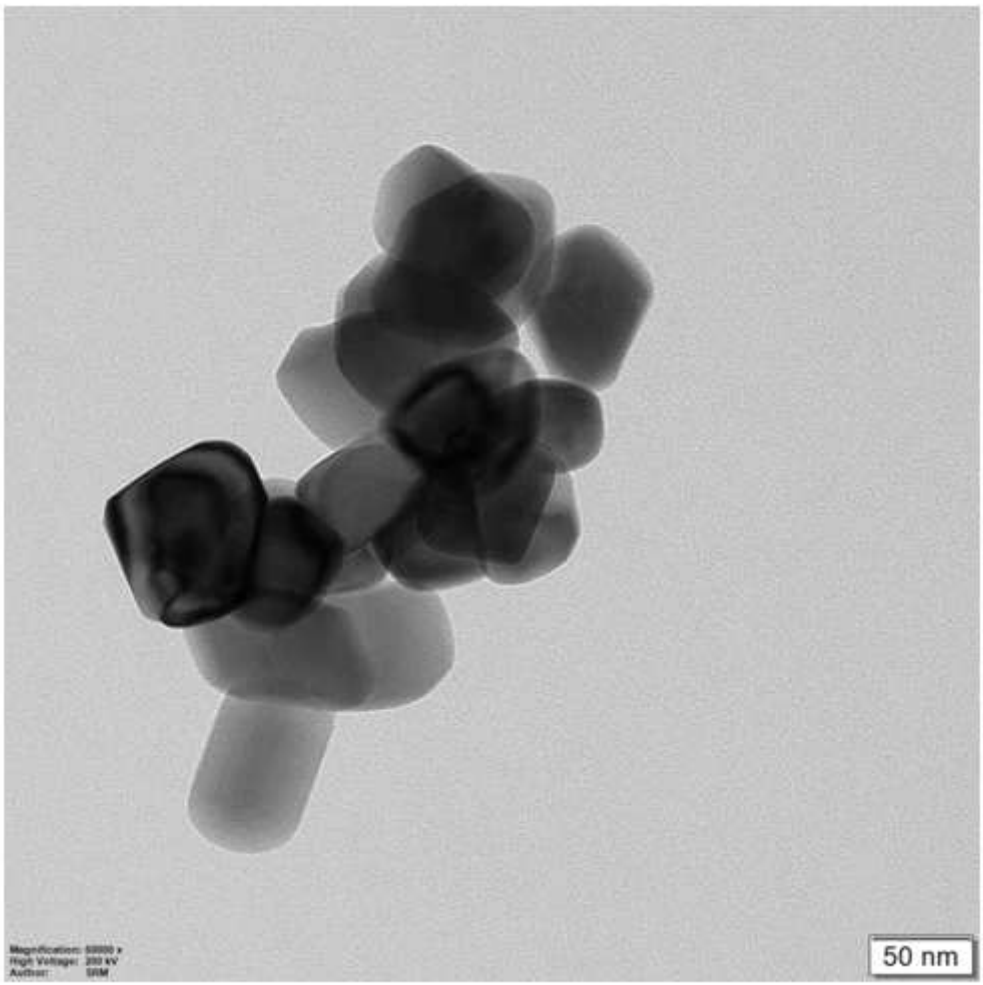

Figure 2

TEM image of 0.5% Er3+ doped BaMoO4 nanostructures

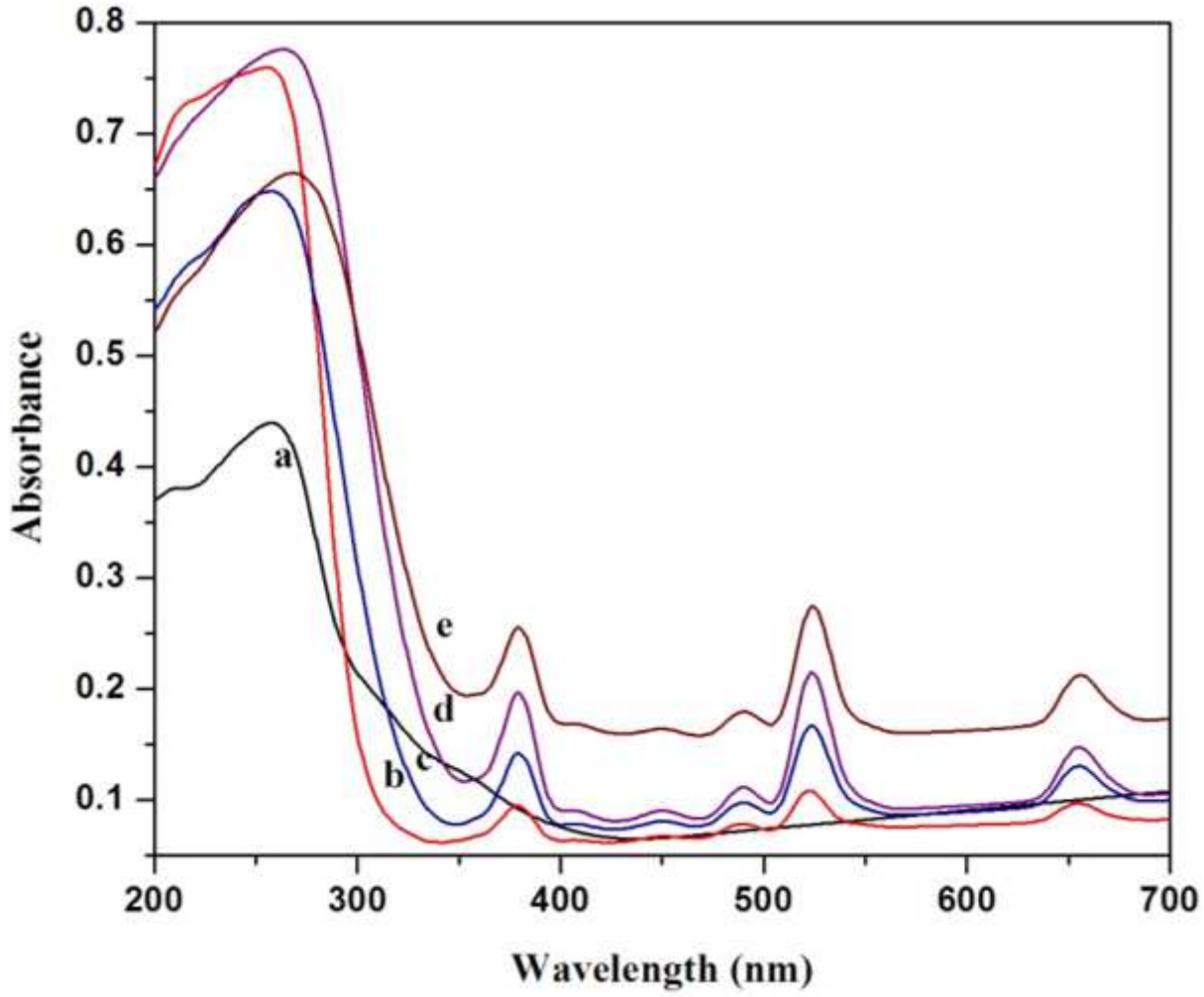

Figure 3

UV-visible spectra of Er3+ doped BaMoO4 nanostructures (a) pure (b) 0.3% (c) 0.5%, (d) 0.7% & (e) 0.9%Er

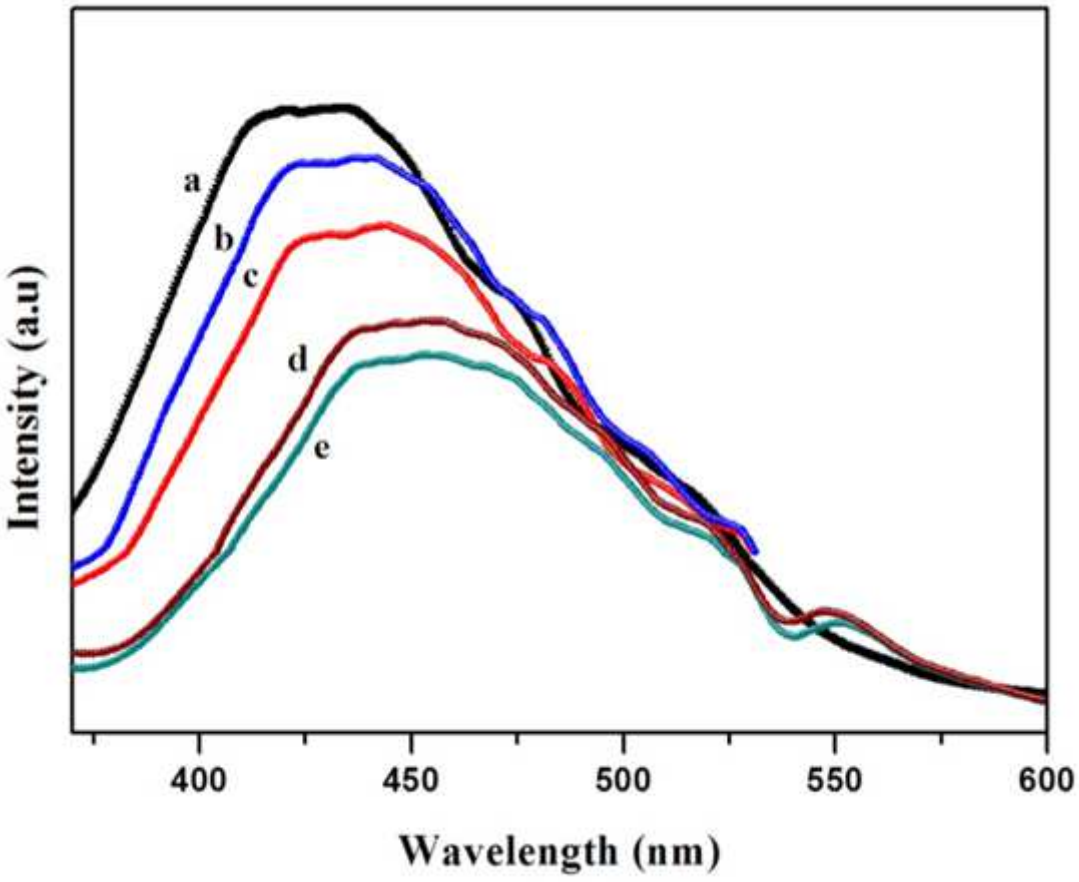

Figure 4

Fluorescence spectra of Er3+ doped BaMoO4 nanostructures (a) pure (b) 0.3% (c) 0.5%, (d) 0.7% & (e) 0.9%Er

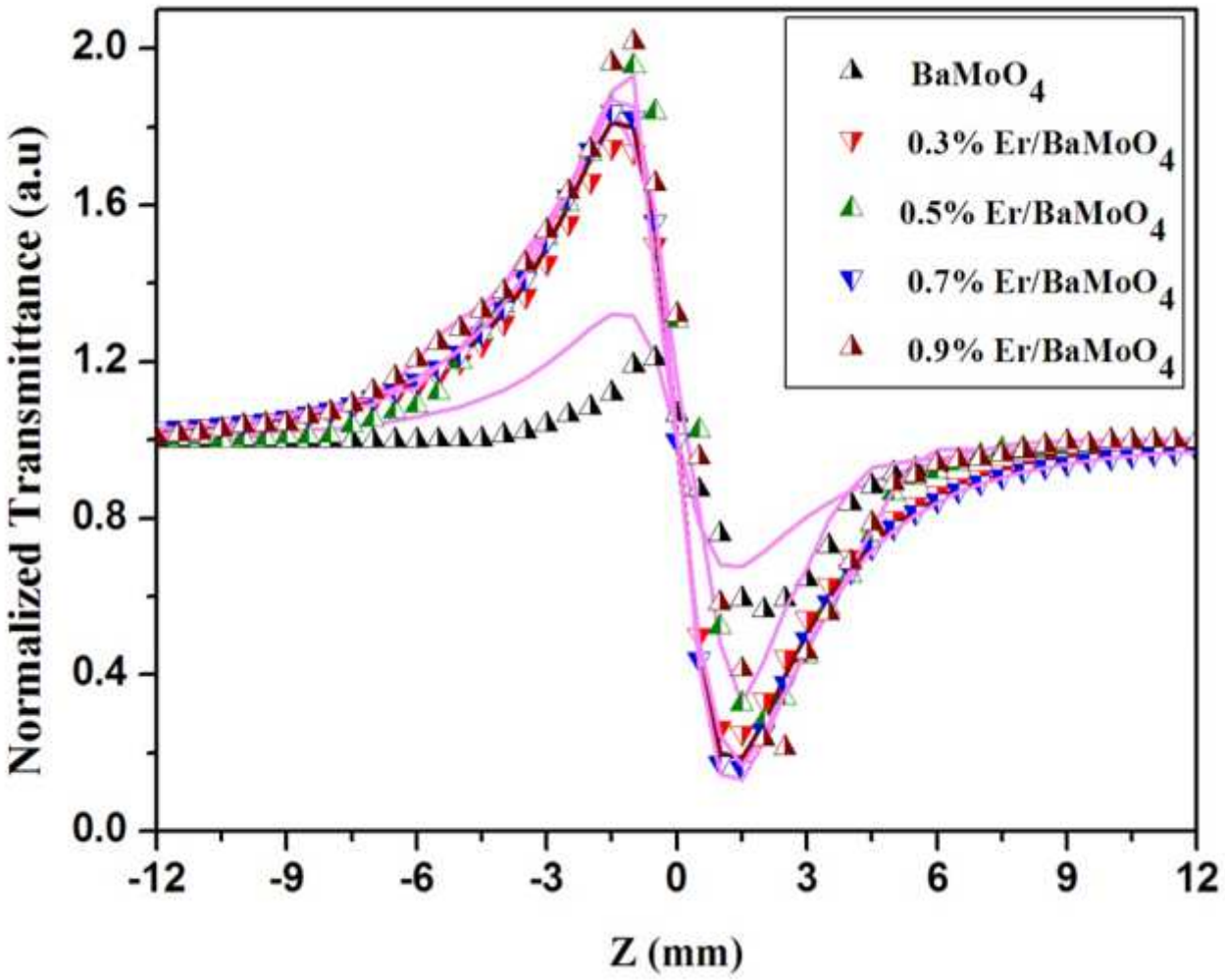

Figure 5

Closed aperture Z-scan data of Er3+ doped BaMoO4 nanostructures

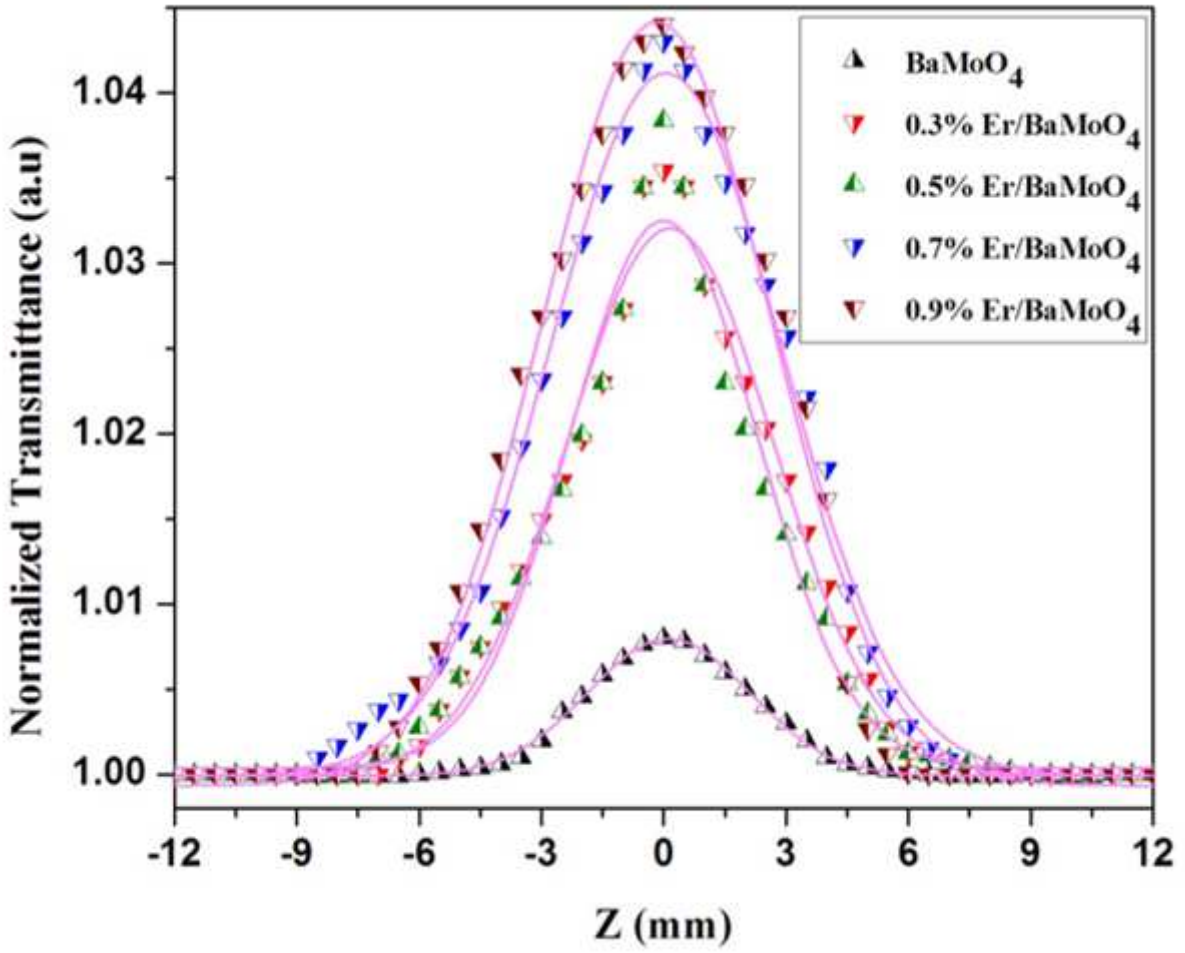

Figure 6

Open aperture Z-scan data of Er3+ doped BaMoO4 nanostructures